

Investigation of some numerical issues in a Chemistry-Transport Model: gas-phase simulations

Vivien Mallet, Adélaïde Pourchet, Denis Quélo and Bruno Sportisse

Cerea: Teaching and Research Center in Atmospheric Environment

Joint Laboratory École Nationale des Ponts et Chaussées (ENPC) /

Électricité de France R&D

<http://www.enpc.fr/cerea/>

Clim: Joint team Inria / École Nationale des Ponts et Chaussées

<http://www-rocq.inria.fr/clime/>

V. Mallet, CEREAs, École Nationale des Ponts et Chaussées, 6-8 Avenue Blaise Pascal, 77455
Champs sur Marne, France. (vivien.mallet@cerea.enpc.fr)

Abstract. Many numerical strategies have been specifically developed for Chemistry-Transport Models. Since no exact solutions are available for 3D real problems, there are only few insights to choose between alternative numerical schemes and approximations, or to estimate the performance discrepancy between two approaches. However it is possible to assess the importance of numerical approximations through the comparison of different strategies. We estimated the impact of several numerical schemes in advection, diffusion and stiff chemistry. We also addressed operator splitting with different methods and operator orders. The study is performed with a gas-phase Eulerian model from the modeling platform POLYPHEMUS. It is applied to ozone forecasts mainly over Europe, with focus on a few key species from a numerical point of view: ozone, nitric oxide, nitrogen dioxide, sulfur dioxide and hydroxy radical. The outcome is a ranking of the most sensitive numerical choices. It stresses the prominent impact of the advection scheme and of the splitting time step.

Introduction

Air Pollution Modeling is based on the so-called Chemistry-Transport Models (CTMs in the sequel; *Seinfeld and Pandis* [1998]; *Jacobson* [2005]). These three-dimensional models solve the Reaction-Diffusion-Advection Partial Differential Equations that describe the time and space evolution of reactive trace species in the atmosphere. They are now widely used for many applications: process study (in order to understand the role of a given physical process), environmental forecast (similar to weather forecast), impact studies (long-term runs in order to evaluate the impact of different scenarios for emissions), inverse modeling of key parameters (on the basis of the coupling between observational data and model outputs),

These models are characterized by their large dimension. Up to hundreds of species have to be taken into account in current comprehensive gas-phase mechanisms (such as *Gery et al.* [1989]; *Stockwell et al.* [1997]). The dimension may be larger for models describing aerosols (particulate matter).

Another key feature of these models is the wide range of spatial and time scales. Many processes occur at micro-physical scales (of magnitude 1 micrometer; for instance, mass transfer) while the characteristic size of grid cells is of magnitude 10 kilometers (or even 100 kilometers) for regional/continental modeling. The range of timescales, especially for chemical reactions, is also wide: from milliseconds for reactive species (radicals) to days or months for more stable species.

As a result of these features, the numerical simulation associated to such models is recognized to be quite difficult. We refer for instance to the monograph *Zlatev* [1995],

to *Sportisse* [2006] or to the primary article *McRae et al.* [1982]. This includes many “classical topics” of numerical analysis, among which

- numerical advection schemes applied to flows with strong gradients (near point sources); the issue related to numerical diffusion is therefore usually underlined.

- operator splitting methods: for many reasons (detailed below), the processes are usually split and appropriate algorithms have to be used to minimize splitting errors.

- time integration of stiff Ordinary Differential Equations: the wide range of chemical timescales implies the stiffness of the resulting equations, and implicit (or at least tailored) algorithms have to be used with a CPU/accuracy trade-off to be optimized.

These issues have often been addressed in the literature since the early 80s. We refer first to the key overview *Verwer et al.* [2002] and to many related works: for instance *Verwer et al.* [1999]; *Sandu et al.* [1997b, a] for stiff solvers and *Lanser and Verwer* [1999]; *Sportisse* [2000] for operator splitting.

Most of these works have been performed in simplified cases, that is to say with simplified gas-phase mechanisms, or in 0D or 1D applications. A key point for 3D atmospheric models is however the large amount of uncertainties in the input data and in the physical parameterizations. These complicated models appear to be highly “stable”: this is not so easy for a change in numerical schemes to drastically modify the outputs of some target species such as ozone (which is a usual concern in gas-phase models).

The key question for a modeler is to know if there is really, among many available algorithms, a “numerical issue”: is there an impact of different numerical strategies in 3D real cases ? Of course, this cannot be answered outside the context of global uncertainties associated to models (including the uncertainties related to data, physical parameteri-

zations and numerics). We refer for instance to *Russell and Dennis* [2000]; *Mallet and Sportisse* [2006a] for a deeper investigation of these points.

The objective of this paper is to briefly review the numerical issues listed above and to try to answer this question. We do not propose new algorithms (apart from specific points) but we perform a comprehensive numerical study of these topics with a real 3D application (air quality modeling mainly over Europe). Even if the tests are made with a specific model, one can expect that the conclusions obtained with our modeling platform can be extended to most of the CTMs.

The focus of this paper is on gas-phase models. The extension to aerosol models is a rather different issue because the numerical simulation of the General Dynamics Equation for aerosol implies other processes with specific numerical behaviors. Moreover, the numerical simulation of aerosols is mainly driven by a coarse discretization (due to the involved computation costs). The extension to aerosol modeling will be the subject of a follower of this paper.

This paper is organized as follows. We briefly describe the Chemistry-Transport Models in the first section. We use the POLYPHEMUS platform [*Mallet et al.*, 2005] to perform the tests. This platform is representative of state-of-the-science numerical tools (used for operational purposes). We also describe the case study: mainly air pollution over Europe for a few days in summer 2001. An evaluation of numerical performance is also described, especially in term of CPU time. We address some issues related to splitting in the second section, to stiffness in the third section (with a focus on positivity), to advection and diffusion in the fourth section.

For the sake of clarity, we have omitted many numerical tests and have only reported the most significant results. In particular, the main results obtained for the regional case (over Northern France, in 1998) are briefly summarized in conclusion.

The complete study related to this article may be found in *Pourchet et al.* [2005].

1. Background and set-up

1.1. Atmospheric dispersion

The time and space evolution of atmospheric trace species is given by the reactive-dispersion equation (*Seinfeld and Pandis* [1998] for instance). For the air concentration c_i of species X_i (the species are labelled by i), the evolution is governed by

$$\frac{\partial c_i}{\partial t} + \text{div}(V(x, t)c_i) = \text{div}(\rho K \nabla \frac{c_i}{\rho}) + \chi_i(c, T(x, t), t) + S_i(x, t) \quad (1)$$

$x \in \mathbf{R}^3$ and t stand for the space and time coordinates, respectively. Notice that the CTMs are usually based on *off-line* coupling with meteorological models. The equations require meteorological inputs that may be

- either direct outputs of meteorological models, such as the wind velocity V , the temperature T or the air density ρ ;
- or parameterized fields such as the eddy diffusivity matrix K , estimated from raw meteorological outputs.

$S_i(x, t)$ represents the volume emissions of species i . The chemical production/loss χ_i for species i is given by a chemical mechanism as a function of kinetic rates and concentrations. The kinetic rates are functions of temperature for thermal reactions and of the actinic flux for photolytic reactions. A key feature is the time dependence of photolysis rates characterized by strong gradients at sunrise and sunset.

Other processes are often added to source terms: scavenging processes (by mass transfer with cloud droplets or rain droplets for soluble species) are usually described by a relaxation term $-\Lambda_i(x, t)c_i$, where Λ_i is a parameterized coefficient.

Boundary conditions (in practice, flux conditions) have to be given at the top of the domain and at ground. At ground, since the vertical wind velocity is zero, they are

$$-\rho K \nabla \frac{c_i}{\rho} \cdot \mathbf{n} = E_i(x, t) - v_i^{dep}(x, t)c_i \quad (2)$$

where \mathbf{n} is the upward unitary vector, E_i the surface emissions and v_i^{dep} the dry deposition velocity, given as a parameterization based on meteorological data and land use cover.

1.2. Numerical platform

The numerical solution is computed by the POLYPHEMUS platform [*Mallet et al.*, 2005]. POLYPHEMUS is a state-of-the-science modeling platform for air quality, that is used both for research projects and operational applications. It is mainly based on

- a library for atmospheric parameterizations and preprocessing of meteorological fields, ATMODATA [*Mallet and Sportisse*, 2005b]; this package computes the physical parameters that appear in the dispersion equation.
- a set of Chemistry-Transport Models (CTMs in the sequel), including POLAIR3D [*Boutahar et al.*, 2004] which used for this work; we assume a CTM is basically a numerical solver for the dispersion equation.
- a postprocessing tool, ATMOPY, in order to perform model-to-data or model-to-model comparisons, and to compute statistics.

POLYPHEMUS is also intended to be used with high-level functionalities, such as sensitivity analysis of model outputs with respect to inputs [*Mallet and Sportisse*, 2005a],

ensemble forecast (multi-models configuration, *Mallet and Sportisse* [2006b]) and data assimilation (coupling between model outputs and observational data, *Quélo et al.* [2005]). A key tool for part of these functionalities is the adjoint model of POLAIR3D [*Mallet and Sportisse*, 2004].

The reference configuration of POLAIR3D used for this work is described thereafter.

The chemical mechanism is RACM [*Stockwell et al.*, 1997], with 72 gas-phase species. The time step is 600 seconds. The reference splitting method is a source splitting method with boundary conditions taken into account in the diffusion. ROS2 (second-order Rosenbrock method) is the scheme for the time integration of chemical kinetics and diffusion; it is solved with $\gamma = 1 + \sqrt{2}/2$ (refer to Section 3) and a time step of 600 seconds. The advection scheme is a third-order Direct Space Time scheme with a Sweby-type flux limiter (Section 4). Besides, the advection is solved without directional splitting. Finally, the diffusion is solved with an horizontal diffusion coefficient K_H set to $10000 \text{ m}^2 \text{ s}^{-1}$ ($5 \text{ m}^2 \text{ s}^{-1}$ at regional scale).

1.3. Case studies

We consider two case studies related to air pollution modeling (photochemistry):

- a continental application over Europe ($[40.25^\circ\text{N}, 10.25^\circ\text{W}] \times [56.75^\circ\text{N}, 22.25^\circ\text{E}]$). The domain is divided into 65 grid cells along x (longitude, grid resolution of 0.5°), 33 grid cells along y (latitude, grid resolution of 0.5°) and 5 grid cells along z, up to 3000 m. This resolution is rather coarse, which is the case in many real applications with CTMs. The timestep is set to 600 s, which is also shared with many CTMs.

- a regional application over Lille (Northern France). The domain is divided into 42 grid cells along x (grid resolution of 0.014°), 44 grid cells along y (grid resolution of 0.009°) and 9 grid cells along z, up to 2780 m . The timestep is set to 600 s.

At continental scale, the lateral boundary conditions come from a global model (Mozart 2 [*Horowitz et al.*, 2003]). At regional scale, the lateral boundary conditions are generated by simulations at continental scale with POLAIR3D.

Unless notified, simulations are performed over seven days. Initial conditions are extracted from a simulation run (1) over several days before the starting date and (2) with the reference configuration. Transient phases are then avoided.

The results are detailed only for the continental scale. The most significant numerical tests for the regional case are briefly summarized in conclusion.

1.4. CPU performances

Numerical choices have an impact on the accuracy, the stability and also on the code CPU performances. In its reference simulation at continental scale, POLAIR3D requires about 5 minutes of CPU time on a Pentium IV (3 Ghz) with Intel Fortan Compiler. In such conditions, we provide below with insights in the schemes costs.

For the continental study, the distribution of most costs (a few functions are excluded such as initialization functions) is the following one: 58.6% of the time is spent in chemistry, 15.2% in advection and 22% in diffusion. Table 1 indicates how computational time is shared within each process. Chemistry has the largest contribution for CPU due to the computation of the kinetic rates (power and exponential functions) and due to linear algebra (linear systems are solved with a LU method).

For the regional study, the distribution is: 10.2% of the time is spent in chemistry, 83.8% in advection and 4.8% in diffusion. The advection appears to be the prominent process. This comes from the *Courant-Friedrichs-Lewy condition* (CFL) $V\Delta t/\Delta x \leq 1$ which implies small sub-timesteps (since the grid cells are smaller than for the continental case) in the advection integration. On average, enforcing the CFL condition requires to perform about X sub-cycles. Note that the sub-cycling never occurs at continental scale where the timestep (600 seconds) is small enough.

A large part of computational time is spent in the numerical flux (52% of total time). Regarding the high CPU time spent in advection, one can wonder whether the advection scheme is well suited. Notice that a significant speed-up can be obtained with other advection schemes, such as a scheme without flux limiter and a basic upwind scheme (see Section 4 for details and the study of accuracy), as indicated in Table 2.

1.5. Procedure for model-to-model comparisons

In order to evaluate the impact of numerics, we have chosen to perform model-to-model comparisons. We assess thereafter, for each process, the spread in the results due to other numerical choices.

A sensitivity analysis is performed to identify the numerical choices that have a strong impact on the results, and those with a minor impact on the computed fields. If strong differences are found between two schemes, the most accurate scheme (the scheme of highest order, for instance) is advocated. If only minor changes arise, the numerical approximation with the lowest computational cost is advocated. We restrict ourselves to ground-level concentrations because this is where concentrations are usually needed and

this is where specific problems arise due to boundary conditions (emissions, deposition velocities).

Let $A = (A_{h,i,j})_{h,i,j}$ and $B = (B_{h,i,j})_{h,i,j}$ be the results of simulations A et B, where h is the temporal index, and i and j label the spatial position. The average over space and time of A is \bar{A} .

The analysis is mostly based on the time evolution of means and standard deviations of concentrations. Another comparison is done with the analysis of all differences between the two simulations. By assuming that an error below 5% can be neglected, a number is derived in order to measure the “distance” between two simulations:

$$a(A, B) = \frac{\text{card}\{(h, i, j) / |\Delta_{h,i,j}| < 5\%\}}{\text{card}\{(h, i, j)\}}, \quad \text{with} \quad \Delta_{h,i,j} = \frac{A_{h,i,j} - B_{h,i,j}}{\frac{1}{2}(\bar{A} + \bar{B})} \quad (3)$$

where card is the cardinal of a set (number of elements). The amount of relative error below 5%, $a(A, B)$, is referred as the *agreement coefficient*. If the agreement coefficient is 100%, the conclusion is that the two simulations are very close. Δ is referred as the *distance* between the two simulations.

An accurate illustration of the differences is the relative frequency distribution D of Δ . It can also be referred as its density and it satisfies

$$\forall \delta \quad \forall \eta > 0$$

$$\int_{[\delta, \delta + \eta]} D(\delta') d\delta' = \frac{\text{card}\{(h, i, j) / \Delta_{h,i,j} \in [\delta, \delta + \eta]\}}{\text{card}\{(h, i, j)\}} \quad (4)$$

where, in practice, η should be large enough to smooth out D . In the sequel, many figures show the relative frequency distribution D (for instance, Figure 2) so that the integral of D over the abscissa range is 0.99.

The following pollutants are studied: ozone (O_3 ; the most studied gas-phase pollutant in photochemistry), nitric oxide (NO; localized at high emission sources), nitrogen dioxide (NO_2), sulfur dioxide (SO_2 ; important for particulate matter and for given emitting sectors) and the hydroxy radical (HO; a key species for the oxidizing power of atmosphere and a species with a very small timescale).

The same accuracy cannot be reached for all species, because of their spatial distribution (strong gradients, e.g. for NO) and their characteristic timescale (much smaller than the numerical timestep, e.g. for HO). It is expected that O_3 and SO_2 are not be strongly affected by a numerical change, notably owing to their quite homogeneous spatial-distribution. Nitric oxide NO is mainly located near emission sources: it is hard to simulate such a species at continental scale. Hydroxy radical is also hard to compute because of its very high reactivity. Nitrogen dioxide NO_2 is intermediate.

To summarize, one can expect that if a numerical change does not affect HO and NO, this change has no impact. If NO_2 concentrations are modified, the numerical change is not negligible. Finally, if concentrations of O_3 and SO_2 are significantly modified (which is measured with the agreement coefficient), the system is sensitive to the numerical change.

In the following sections, we first briefly summarize the background and the algorithms and then discuss the results of the numerical tests applied to the continental case study.

2. Splitting methods

2.1. Background

Let us consider Equation 1. We suppose that the model relies on a finite-volume framework for spatial discretization (which is usually the case for CTMs): the model computes

cell-averaged values. Let n_s be the number of chemical species and n_g the number of grid cells (usually greater than 10,000).

Using a coupled algorithm for the integration of such a Partial Differential Equation is quite difficult for at least three reasons:

- there is a growing use of parameterizations, couplings, feedbacks that make black boxes attractive;
- as far as modularity is concerned (a strong request in *Carmichael et al.* [1996]; *Peters et al.* [1995]), it is better to use appropriate solvers and then to solve independently the phenomena to be taken into account;
- as far as CPU time is concerned, if we use the Method of Lines (first discretize with respect to space and then integrate the resulting ODEs – Ordinary Differential Equations), the ODEs to be integrated have a dimension $n_g \times n_s$. These ODEs are stiff (see below) and implicit methods are usually advocated. The complexity of matrix “inversions” (with a LU method) is then of magnitude $O((n_g n_s)^3)$.

Operator splitting methods are then commonly advocated in this context [*McRae et al.*, 1982; *Verwer et al.*, 2002; *Sportisse*, 2000]. The dispersion equation is then viewed as a sequence of three main processes:

- Advection:

$$\frac{\partial c_i}{\partial t} = -\text{div}(V(x, t)c_i) \quad (5)$$

- Turbulent diffusion:

$$\frac{\partial c_i}{\partial t} = \text{div}(\rho K \nabla \frac{c_i}{\rho}) \quad (6)$$

- Chemical reactions and source terms:

$$\frac{\partial c_i}{\partial t} = \chi_i(c, T(x, t), t) + S_i(x, t) \quad (7)$$

with appropriate boundary conditions, when required. In practice, ground boundary conditions (Equation 2) are integrated with diffusion, and, in advection, zero inflow and outflow fluxes are assumed at ground.

The classical methods and the corresponding numerical analysis are usually given in the linear case:

$$\frac{dc}{dt} = Ac + Bc, c(0) = c_n \quad (8)$$

A and B are two linear operators. The concentration c_n is current value of the solution at time $t_n = n\Delta t$ where Δt is the so-called splitting time step. The splitting algorithm computes an estimation c_{n+1} of the solution c at time $t_{n+1} = t_n + \Delta t$.

2.1.1. First-order methods

The simplest splitting method is of course:

- First step: integrate operator A

$$\frac{dc^*}{dt} = Ac^* \quad \text{over } [0, \Delta t], c^*(0) = c_n \quad (9)$$

- Second step: integrate operator B

$$\frac{dc^{**}}{dt} = Bc^{**} \quad \text{over } [0, \Delta t], c^{**}(0) = c^*(\Delta t) \quad (10)$$

We write $c^*(\Delta t) = L_{[0, \Delta t]}^A(c_n)$ and $c^{**}(\Delta t) = L_{[0, \Delta t]}^B(c^*(\Delta t))$. The approximation of $c(\Delta t)$ is then $c_{n+1} = L_{[0, \Delta t]}^B L_{[0, \Delta t]}^A(c_n)$.

The classical analysis for this method is based on asymptotic expansions with respect to the splitting time step Δt supposed to be small. We have then a first-order method

unless A and B are commuting operators (in this case the splitting error is 0 since the exponential operators commute). The extension of such an analysis to the nonlinear case may be performed by using the notion of Lie derivative (*Lanser and Verwer* [1999] for instance).

2.1.2. Second-order methods

Strang [*Strang*, 1968] has proposed to symmetrize the previous method with the following three steps:

- First step: integrate A over $[0, \frac{\Delta t}{2}]$ from c_n ;
- Second step: integrate B over $[0, \Delta t]$;
- Third step: integrate A over $[\frac{\Delta t}{2}, \Delta t]$.

The approximation of $c(\Delta t)$ is then $c_{n+1} = L_{[\Delta t/2, \Delta t]}^A L_{[0, \Delta t]}^B L_{[0, \Delta t/2]}^A(c_n)$.

This is a second-order method unless operators commute. We refer to *Sportisse* [2000] for the analysis of order reduction and the investigation of the optimal sequence in the stiff case (when one operator is chemical kinetics, for instance).

2.1.3. Internal splitting

A different approach is to perform the splitting process at the level of linear algebra. This is sometimes referred as *internal splitting* (see *Verwer et al.* [1996a] for instance).

Let us use an implicit method (for instance Backward Euler) in order to compute the solution of Equation 8: $(I - (A + B)\Delta t)c_{n+1} = c_n$.

The key idea of internal splitting is then to propose an approximate factorization of the matrix to be inverted. For instance, if we choose $I - (A + B)\Delta t \simeq (I - A\Delta t)(I - B\Delta t)$, this leads to the sequential integration of $(I - A\Delta t)c^* = c_n$ and $(I - B\Delta t)c^{**} = c^*$. A

similar method has been proposed in another context for Navier-Stokes equations [*Perot*, 1993] where splitting methods are interpreted as approached LU factorizations of matrices.

2.1.4. Source splitting methods

In order to avoid the transient phases introduced by operator splitting methods (due to the change of initial conditions for each step; see *Sportisse* [2000]) alternative methods have been proposed in *Sun* [1996] (no time splitting) and in *Knoth and Wolke* [1994] (source splitting).

The key idea is to avoid this change of initial conditions by adding artificial terms. Let us assume that B is a stiff operator (chemical kinetics). In order to avoid a transient phase during the integration of B , a slight modification of the first-order method is recommended (with the sequence $A - B$):

- First step: integrate operator A , $c^*(\Delta t) = L_{[0, \Delta t]}^A(c_n)$.
- Second step: integrate operator B with a complementary source term

$$\frac{dc^{**}}{dt} = Bc^{**} + \frac{c^*(\Delta t) - c_n}{\Delta t} \quad \text{on } [0, \Delta t], \text{ with } c^{**}(0) = c_n. \quad (11)$$

Notice that the initial condition for the second step has not been modified. A classical analysis of this method proves that this a first-order method. The key point is that transient phases have been eliminated [*Sportisse*, 2000]. A stability analysis of this algorithm coupled with Rosenbrock methods can be found in *Verwer et al.* [1999]. Even if there is a lack of $A(\alpha)$ stability, this algorithm appears to be stable in practice. It also has many common points with implicit-explicit methods [*Ahmad and Berzins*, 1997; *Ascher et al.*, 1995; *Berzins and Ware*, 1996; *Frank et al.*, 1997; *Verwer et al.*, 1996a; *Knoth and Wolke*, 1998; *Wolke and Knoth*, 2000; *Knoth and Wolke*, 1999].

2.1.5. Splitting of boundary conditions

The key point is to choose in which process to include them. As a reference, POLAIR3D solves the ground boundary conditions (Equation 2) with diffusion. An alternative is to add these boundary conditions as sources for chemistry, which is possible owing to the finite volume framework of the model.

2.2. Numerical tests

2.2.1. Sequence of processes within the splitting

In the reference simulation, the splitting sequence is: advection, diffusion and then chemistry (ADC). This sequence is chosen so as to put the stiffest operator at the end, as advocated in *Sportisse* [2000]. Ground boundary conditions (emissions and deposition velocities) are integrated with diffusion.

The tests show that the key point is the position (in the sequence) of chemistry with respect to diffusion. Simulations in which chemistry is integrated after diffusion (ADC, DCA and DAC) compute (almost) the same concentrations. In the same way, simulations in which diffusion is integrated after chemistry (ACD, CDA and CAD) deliver very similar results. These results are illustrated in Figure 1.

A finer analysis shows slight differences between the simulations in which chemistry and diffusion are kept in the same order (see Figure 2). Nevertheless, when chemistry and diffusion are switched, the agreement between the simulations clearly decreases (see Figure 3). The key point therefore lies in the relative position (in the sequence) of chemistry and diffusion, as shown in *Sportisse* [2000].

2.2.2. Boundary conditions

Ground boundary conditions are included in diffusion. The sensitivity to the chemistry/diffusion sequence may come from these boundary conditions. Figure 4 shows that this is not the main reason. With ground boundary conditions moved to chemistry, the differences are not as high as previously, except for ozone. Meanwhile ozone concentrations are not strongly modified. As a conclusion, the impact of this choice about the ground boundary conditions is not negligible but it does not explain the impact of the splitting sequence.

2.2.3. Splitting method

The use of the method described in section 2.1.2 has a slight impact on concentrations, as shown in Figure 5.

The impact of a change from first-order splitting to internal splitting (Section 2.1.3) is still low for ozone and sulfur dioxide. Other species show differences, but lower than in the previous tests. Results are summarized in Figure 6.

As for the impact of source splitting (Section 2.1.4), concentrations are slightly modified (Figure 7). Nevertheless, this method improves the stability of the integration. Without source splitting, instabilities occur with large time steps such as 1800 s.

2.2.4. Splitting time step

The choice of the splitting time step (also referred as time step) is crucial because the overall computational time is roughly proportional to it. CTMs use time steps higher than the time scales of many chemical reactions. Moreover, there are advection schemes without a CFL restriction [*Hundsdofer and Spee*, 1995; *Frolkovič*, 2002; *Lin and Rood*, 1996; *Restelli et al.*, 2006]. Time steps may therefore vary in a wide range, maybe up to one hour (which is still reasonable for the dynamics).

We have used time steps of 30 s, 60 s, 100 s, 200 s, 300 s, 600 s, 900 s, 1200 s and 1800 s. All results are similar up to 600 s. With time steps above 600 s, the results show noteworthy differences (see Figure 8).

2.2.5. Conclusion

The main conclusions are

1. The splitting time step (up to 600 s) and the scheme order do not make much of a difference. Using a first-order method with a splitting time step of 600 seconds is then a good compromise between CPU requirements and accuracy. Source splitting should be used to improve the stability (without additional CPU costs).

2. The sequence of processes reveals an impact of the position of chemistry and diffusion in the sequence; chemistry should end the sequence.

3. The impact of boundary conditions integrated with chemistry (instead of diffusion) remains limited.

3. Integration of chemical kinetics

3.1. Background

The time integration of chemical kinetics is usually a key step for gas-phase CTMs. The reasons are twofold:

- many species are included in comprehensive chemical mechanisms (72 species in the case of the RACM mechanism used in POLYPHEMUS, *Stockwell et al.* [1997]). This leads to high-dimensional models with the related difficulties.

- the wide range of chemical timescales implies the numerical stiffness of the ODEs [Verwer *et al.*, 1996b; Verwer, 1994; Verwer and Simpson, 1995; Sandu *et al.*, 1997b, 1996, 1997b].

The classical issues of stiff ODEs have therefore to be dealt with

- implicit methods instead of explicit ones in order not to be constrained by stringent stability conditions;

- positivity of concentrations, especially to keep the property of stability for chemical kinetics. If the positivity is not satisfied, clipping is applied: the negative concentrations are set to zero. This is widely used (even if this leads to mass addition). An alternative is the use of tailored solvers (such as Preussner and Brand [1981]). We also refer to Sandu [2001] for an appropriate algorithm.

Among many candidates, the Rosenbrock methods (Verwer *et al.* [1999] for gas-phase mechanisms and Djouad *et al.* [2002] for multi-phase models) have appeared to have good skills. For the evolution equation,

$$\frac{dc}{dt} = f(c, t), \quad c(0) = c_0 \quad (12)$$

the second-order Rosenbrock method (ROS2) reads

$$c_{n+1} = c_n + (3k_1 + k_2) \frac{\Delta t}{2} \quad (13)$$

where

$$(1 - \gamma \Delta t J)k_1 = f(t_n, c_n), \quad (1 - \gamma \Delta t J)k_2 = f(t_{n+1}, c_n + \Delta t k_1) - 2k_1 \quad (14)$$

J is an approximation of the Jacobian matrix $\partial f / \partial c$. The parameter γ is equal to $1 + \sqrt{2}/2$ to ensure stability (L-stability, see below).

In this section, we focus on the positivity of the concentration. A key point is related to sunset and sunrise. Usually, the linear(ized) system with $f(c) = -\lambda c$ ($\lambda > 0$) is studied. In order to reproduce sunset or sunrise, we introduce a parameter β such that $f(c, t_n) = -\lambda c$ and $f(c, t_{n+1}) = -\beta\lambda c$: $\beta > 1$ for sunrise and $\beta < 1$ for sunset.

One easily gets the stability function in this case:

$$R(\lambda) = \frac{(2\gamma^2 - (3 + \beta)\gamma + \beta)\lambda^2 + (4\gamma - 1 - \beta)\lambda + 2}{2(1 + \gamma\lambda)^2} \quad (15)$$

One way to get the L-stability (i.e. $\lim_{\lambda \rightarrow +\infty} R(\lambda) = 0$) is to take $\gamma(\beta)$ as the root of the second-order algebraic equation $2\gamma^2 - (3 + \beta)\gamma + \beta = 0$. Since $(3 + \beta)^2 - 8\beta > 0$, there are two roots: $\gamma^\pm(\beta) = (3 + \beta \pm \sqrt{\beta^2 - 2\beta + 9})/4$.

Note that, in the autonomous case (i.e., $\beta = 1$), $\gamma^+ = 1 + \sqrt{2}/2$, which is the reference value. With $\gamma^+(\beta)$, the stability function becomes

$$R(\lambda) = \frac{(2 + \sqrt{\beta^2 - 2\beta + 9})\lambda + 2}{2(1 + \gamma^+\lambda)^2} \quad (16)$$

Since λ is positive, we have $R(\lambda) \geq 0$, and the scheme is therefore positive. In practice, $\gamma^+(\beta)$ is computed by calculating the Jacobian matrix at time t_{n+1} with the same concentrations but with updated photolysis rates. The estimation of $\gamma^+(\beta)$ is then given by the highest ratio of the diagonal values between t_n and t_{n+1} .

3.2. Numerical tests

3.2.1. Influence of Δt

The chemistry may have its own time step (sub-cycling within the splitting sequence). We have tried different time steps for the chemistry, i.e. 30 s, 60 s, 100 s, 200 s, 300 s and 600 s. No impact is found.

3.2.2. Clipping

First a diagnosis of clipped values is necessary to check whether this may be an issue. The mass added to the system is shown in Table 3 with the ratio of clipped concentrations and mean concentrations. A few species (among the 72 species of the chemical mechanism) are associated with significant ratios. We refer to *Stockwell et al.* [1997] for the nomenclature of species. Nevertheless, strong corrections may appear at sunrise and sunset, that is in cases where the system is highly non-autonomous (because of photolysis rates). Table 4 shows the maximum ratio between clipped concentrations and mean concentrations. There are very high ratios.

3.2.3. Influence of γ

Highly clipped concentrations appear at sunrise, when photolysis rates increase, that is when $\beta > 1$ (Section 3.1). In this case, $\gamma > 1 + \sqrt{2}/2$. Indeed, higher values of γ decrease clipped concentrations, as shown in Figure 9. Meanwhile the impact on the concentrations is low (see Figure 10). Higher values are however not advocated since it may lead to instabilities. For instance, with $\gamma = 5$, the simulation is unstable. In addition, since the changes are negligible for the main species (O_3 , SO_2 , even NO_2), the new value of γ does not bring much improvements to the simulation results.

With $\gamma = \gamma^+(\beta)$, the results are not improved (Figure 11). The approximation of β (maximum ratio of the values on the diagonals of Jacobian matrices) is probably too coarse.

3.2.4. Conclusion

Concentrations are mainly clipped at sunrise, when the system is non-autonomous due to increasing photolysis-rates. Nevertheless clipped concentrations remain low, except in

a few cases. As for the value of γ , the classical choice seems to be a good compromise which ensures stability.

4. Advection and diffusion

4.1. Background

There are many issues related to advection, including

- mass conservation;
- numerical diffusion: this is a crucial point, especially for accidental releases in a clean atmosphere (strong gradients near the sources).

For the sake of clarity, we only present the algorithms for the mono-dimensional case:

$$\frac{\partial c}{\partial t} + \frac{\partial(uc)}{\partial x} = 0, \tag{17}$$

where u is the wind velocity. Let Δt be the time step and Δx the grid size. We define $t_n = n\Delta t$ and $x_{i-1/2} = (i - 1/2)\Delta x$. Let c_i^n be the numerical value of c at t_n in the cell $[x_{i-1/2}, x_{i+1/2}]$. The conservative form of the numerical scheme is

$$c_i^{n+1} = c_i^n + F_{i-1/2}^n - F_{i+1/2}^n, \tag{18}$$

with $F_{i-1/2}^n$ the numerical flux at $x_{i-1/2}$.

The key focus of this section is to investigate if high-order schemes and flux limiters are required. Three algorithms are then compared:

1. the upwind scheme (positive but diffusive):

$$F_{i+1/2} = \begin{cases} \nu_{i+1/2} c_i & \text{if } u_{i+1/2} \geq 0 \\ -\nu_{i+1/2} c_{i+1} & \text{if } u_{i+1/2} < 0 \end{cases} \tag{19}$$

2. a third-order scheme without flux limiter (little diffusive, but not positive; *Spee* [1998]):

$$F_{i+1/2} = \begin{cases} \nu_{i+1/2} \left(c_i + d_0(\nu_{i+1/2})(c_{i+1} - c_i) + d_1(\nu_{i+1/2})(c_i - c_{i-1}) \right) & \text{if } u_{i+1/2} \geq 0 \\ -\nu_{i+1/2} \left(c_{i+1} + d_0(\nu_{i+1/2})(c_i - c_{i+1}) + d_1(\nu_{i+1/2})(c_{i+1} - c_{i+2}) \right) & \text{if } u_{i+1/2} < 0 \end{cases} \quad (20)$$

3. the same third-order scheme, with a Sweby-type flux limiter (intermediate; *Verwer et al.* [2002]), which is the reference scheme of POLAIR3D:

$$F_{i+1/2} = \begin{cases} \nu_{i+1/2} \left(c_i + \psi \left(\nu_{i+1/2}, \theta_i \right) (c_{i+1} - c_i) \right) & \text{if } u_{i+1/2} \geq 0 \\ -\nu_{i+1/2} \left(c_{i+1} + \psi \left(\nu_{i+1/2}, \frac{1}{\theta_{i+1}} \right) (c_i - c_{i+1}) \right) & \text{if } u_{i+1/2} < 0 \end{cases} \quad (21)$$

where $u_{i+1/2} \simeq u(x_{i+1/2}, t_n)$ and $\nu_{i+1/2} = |u_{i+1/2}| \frac{\Delta t}{\Delta x}$ is the CFL number. The limiter function is

$$\psi(\nu, \theta) = \max \left(0, \min \left(1, d_0(\nu) + d_1(\nu)\theta, \frac{1-\nu}{\nu}\theta \right) \right). \quad (22)$$

with

$$d_0(\nu) = \frac{1}{6}(2-\nu)(1-\nu), \quad d_1(\nu) = \frac{1}{6}(1-\nu^2), \quad \theta_i = \frac{c_i - c_{i-1}}{c_{i+1} - c_i} \quad (23)$$

For this scheme, the CFL condition is $\nu_{i+1/2} \leq 1$.

4.2. Numerical test

A strong impact of the advection scheme is found. The first-order upwind scheme is so diffusive that its agreement coefficient with the reference simulation (third-order scheme with flux limiter) falls to 66% for ozone. Figure 12 illustrates the results.

There are less differences between the reference scheme and the third-order scheme (without flux limiter), but the impact is still high. Figure 13 shows the results.

4.3. Impact of horizontal diffusion

The horizontal diffusion coefficient is not a well known physical parameter. It is sometimes set to zero because the advection scheme introduces numerical diffusion. In order to assess the impact of the coefficient, three simulations are performed with the following horizontal diffusion coefficients: $K_h = 0 \text{ m}^2 \text{ s}^{-1}$, $K_h = 10,000 \text{ m}^2 \text{ s}^{-1}$ and $K_h = 50,000 \text{ m}^2 \text{ s}^{-1}$.

Spatial means of output concentrations are not affected by the coefficient. As expected, maxima and (spatial) standard deviations are clearly modified when $K_h = 50,000 \text{ m}^2 \text{ s}^{-1}$ and somewhat modified for $K_h = 10,000 \text{ m}^2 \text{ s}^{-1}$. Figure 14 shows the impacts on the standard deviation.

Conclusion

In this article we have investigated some numerical issues for Chemistry-Transport Models with the use of the POLYPHEMUS platform and model-to-model comparisons. Table 5 gathers the main results. One can conclude that the time step should not be increased above 600 s, that the choice of the advection scheme is a key point, that the horizontal diffusion coefficient may have a strong impact for high horizontal diffusions. Issues related to operator splitting are less prominent.

The results obtained at continental scale can not be directly transposed to the regional case (see Table 6). For instance, the time step has better to be small enough to avoid splitting errors.

Further conclusions should take into account the purpose of the simulations. The model species are not sensitive to the same numerical choices. For a given species, the impact

may be high on the maxima but not on averaged concentrations. Previous conclusions are mainly drawn for hourly ozone concentrations.

Numerical schemes are source of errors and therefore of uncertainties. Nevertheless, this uncertainty should be compared to the uncertainty due to coarse input data or due to physical parameterizations. For instance, in *Mallet and Sportisse* [2006a], it is shown that the relative uncertainty on ozone concentrations is higher than 16% (relative standard deviation), which is clearly above the impact of numerical schemes.

References

- Ahmad, I., and M. Berzins, An algorithm for ODEs from atmospheric dispersion problems, *Appl. Numer. Math.*, 25(2–3), 137–149, 1997.
- Ascher, U., S. Ruuth, and B. Wetton, Implicit-explicit methods for time-dependent partial differential equations, *SIAM J. Numer. Anal.*, 32(3), 797–823, 1995.
- Berzins, M., and J. M. Ware, Solving convection and convection-reaction problems using the method of lines, *Appl. Numer. Math.*, 20(1–2), 83–99, 1996.
- Boutahar, J., S. Lacour, V. Mallet, D. Quélo, Y. Roustan, and B. Sportisse, Development and validation of a fully modular platform for numerical modelling of air pollution: POLAIR, *Int. J. Env. and Pollution*, 22(1/2), 17–28, 2004.
- Carmichael, G. R., A. Sandu, F. Potra, V. Damian, and M. Damian, The current state and the future directions in air quality modeling, *SAMS*, 25, 75–105, 1996.
- Djouad, R., B. Sportisse, and N. Audiffren, Numerical simulation of aqueous-phase atmospheric models: use of a non-autonomous Rosenbrock method, *Atmos. Env.*, 36(5), 873–879, 2002.

- Frank, J., W. Hundsdorfer, and J. G. Verwer, On the stability of implicit-explicit linear multistep methods, *Appl. Numer. Math.*, 25(2–3), 193–205, 1997.
- Frolkovič, P., Flux-based method of characteristics for contaminant transport in flowing groundwater, *Comp. and Vis. Sci.*, 5(2), 73–83, 2002.
- Gery, M. W., G. Z. Whitten, J. P. Killus, and M. C. Dodge, A photochemical kinetics mechanism for urban and regional scale computer modeling, *J. Geophys. Res.*, 94, 12,925–12,956, 1989.
- Horowitz, L. W., et al., A global simulation of tropospheric ozone and related tracers: description and evaluation of MOZART, version 2, *J. Geophys. Res.*, 108(D24), 2003.
- Hundsdorfer, W., and E. Spee, An efficient horizontal advection scheme for the modeling of global transport of constituents, *Mon. Wea. Rev.*, 123(12), 3,554–3,564, 1995.
- Jacobson, M. Z., *Fundamentals of Atmospheric Modeling*, second ed., Cambridge University Press, 2005.
- Knoth, O., and R. Wolke, *Air pollution modelling and its applications X*, chap. A comparison of fast chemical kinetic solvers in a simple vertical diffusion model, Plenum Press, 1994.
- Knoth, O., and R. Wolke, An explicit-implicit numerical approach for atmospheric chemistry-transport modeling, *Atmos. Env.*, 32(10), 1,785–1,797, 1998.
- Knoth, O., and R. Wolke, Strang splitting versus implicit-explicit methods in solving chemistry transport models, in *Proceedings EUROTRAC symposium '98*, vol. 2, edited by P. M. Borrell and P. Borrell, WIT-press, 1999.
- Lanser, D., and J. G. Verwer, Analysis of operator splitting for advection-diffusion-reaction problems from air pollution modelling, *J. Comp. Appl. Math.*, 111, 201–216,

1999.

Lin, S.-J., and R. B. Rood, Multidimensional flux-form semi-Lagrangian transport schemes, *Mon. Wea. Rev.*, *124*(9), 2,046–2,070, 1996.

Mallet, V., and B. Sportisse, 3-D chemistry-transport model Polair: numerical issues, validation and automatic-differentiation strategy, *Atmos. Chem. Phys. Discuss.*, *4*, 1,371–1,392, 2004.

Mallet, V., and B. Sportisse, A comprehensive study of ozone sensitivity with respect to emissions over Europe with a chemistry-transport model, *J. Geophys. Res.*, *110*(D22), 2005a.

Mallet, V., and B. Sportisse, Data processing and parameterizations in atmospheric chemistry and physics: the AtmoData library, *Tech. Rep. 12*, CEREAs, 2005b.

Mallet, V., and B. Sportisse, Uncertainty in a chemistry-transport model due to physical parameterizations and numerical approximations: An ensemble approach applied to ozone modeling, *J. Geophys. Res.*, *111*(D1), 2006a.

Mallet, V., and B. Sportisse, Ensemble-based air quality forecasts: A multimodel approach applied to ozone, *J. Geophys. Res.*, *111*, 2006b.

Mallet, V., D. Quélo, and B. Sportisse, Software architecture of an ideal modeling platform in air quality – A first step: Polyphemus, *Tech. Rep. 11*, CEREAs, 2005.

McRae, G. J., W. R. Goodin, and J. H. Seinfeld, Numerical solution of the atmospheric diffusion equation for chemically reactive flows, *J. Comp. Phys.*, *45*, 1–42, 1982.

Perot, J. B., An analysis of the fractional step method, *J. Comp. Phys.*, *108*(1), 51–58, 1993.

- Peters, L. K., et al., The current state and future direction of Eulerian models in simulating the tropospheric chemistry and transport of trace species: a review, *Atmos. Env.*, *29*(2), 189–222, 1995.
- Pourchet, A., V. Mallet, D. Quélo, and B. Sportisse, Some numerical issues in Chemistry-Transport Models – a comprehensive study with the Polyphemus/Polair3D platform, *Tech. Rep. 26*, CEREIA, 2005.
- Preussner, P. R., and K. P. Brand, Application of a semi-implicit Euler method to mass action kinetics, *Chem. Eng. Sci.*, *36*(10), 1,633–1,641, 1981.
- Quélo, D., V. Mallet, and B. Sportisse, Inverse modeling of NO_x emissions at regional scale over northern France: Preliminary investigation of the second-order sensitivity, *J. Geophys. Res.*, *110*(D24), 2005.
- Restelli, M., L. Bonaventura, and R. Sacco, A semi-Lagrangian discontinuous Galerkin method for scalar advection by incompressible flows, *J. Comp. Phys.*, *216*(1), 195–215, 2006.
- Russell, A., and R. Dennis, NARSTO critical review of photochemical models and modeling, *Atmos. Env.*, *34*, 2,283–2,234, 2000.
- Sandu, A., Positive numerical integration methods for chemical kinetic systems, *J. Comp. Phys.*, *170*(2), 589–602, 2001.
- Sandu, A., F. A. Potra, G. R. Carmichael, and V. Damian, Efficient implementation of fully implicit methods for atmospheric chemical kinetics, *J. Comp. Phys.*, *129*, 101–110, 1996.
- Sandu, A., J. G. Verwer, J. G. Blom, E. J. Spee, G. R. Carmichael, and F. A. Potra, Benchmarking stiff ODE solvers for atmospheric chemistry problems II: Rosenbrock

- solvers, *Atmos. Env.*, *31*(20), 3,459–3,472, 1997a.
- Sandu, A., J. G. Verwer, M. V. Loon, G. R. Carmichael, F. A. Potra, D. Dabdub, and J. H. Seinfeld, Benchmarking stiff ODE solvers for atmospheric chemistry problems-I. Implicit vs explicit, *Atmos. Env.*, *31*(19), 3,151–3,166, 1997b.
- Seinfeld, J. H., and S. N. Pandis, *Atmospheric chemistry and physics: from air pollution to climate change*, Wiley-Interscience, 1998.
- Spee, E. J., Numerical methods in global transport-chemistry models, Ph.D. thesis, University of Amsterdam, 1998.
- Sportisse, B., An analysis of operator splitting techniques in the stiff case, *J. Comp. Phys.*, *161*(1), 140–168, 2000.
- Sportisse, B., A review of current issues in air pollution modeling and simulation, *J. Comp. Geosci.*, accepted for publication, 2006.
- Stockwell, W. R., F. Kirchner, M. Kuhn, and S. Seefeld, A new mechanism for regional atmospheric chemistry modeling, *J. Geophys. Res.*, *102*(D22), 25,847–25,879, 1997.
- Strang, G., On the construction and comparison of difference schemes, *SIAM J. Numer. Anal.*, *5*(3), 506–517, 1968.
- Sun, P., A pseudo-non-time-splitting method in air quality modeling, *J. Comp. Phys.*, *127*, 152–157, 1996.
- Verwer, J. G., Gauss-Seidel iteration for stiff ODES from chemical kinetics, *SIAM J. Sci. Comp.*, *15*(5), 1,243–1,250, 1994.
- Verwer, J. G., and D. Simpson, Explicit methods for stiff ODEs from atmospheric chemistry, *Appl. Numer. Math.*, *18*(1–3), 413–430, 1995.

- Verwer, J. G., J. G. Blom, and W. Hundsdorfer, An implicit-explicit approach for atmospheric transport-chemistry problems, *Appl. Numer. Math.*, *20*, 191–209, 1996a.
- Verwer, J. G., J. G. Blom, M. van Loon, and E. J. Spee, A comparison of stiff ODE solvers for atmospheric chemistry problems, *Atmos. Env.*, *30*(1), 49–58, 1996b.
- Verwer, J. G., E. J. Spee, J. G. Blom, and W. Hundsdorfer, A second-order Rosenbrock method applied to photochemical dispersion problems, *SIAM J. Sci. Comp.*, *20*(4), 1,456–1,480, 1999.
- Verwer, J. G., W. Hundsdorfer, and J. G. Blom, Numerical time integration for air pollution models, *Surveys on Math. for Indus.*, *10*, 107–174, 2002.
- Wolke, R., and O. Knöth, Implicit-explicit Runge-Kutta methods applied to atmospheric chemistry-transport modelling, *Env. Mod. Soft.*, *15*(6–7), 711–719, 2000.
- Zlatev, Z., *Computer treatment of large air pollution models*, Kluwer Academic Publishers, 1995.

Table 1. Distribution of CPU time for the continental and regional cases (reference configuration).

Process	Continental case	Regional case
Chemistry	58.6 %	10.2 %
incl. kinetic rates	incl. 16.3 %	
incl. LU decomposition	incl. 16.8 %	
Advection	15.2 %	83.8 %
incl. flux limiting	incl. 9.3 %	incl. 52.2 %
Diffusion	22 %	4.8 %
incl. vertical diffusion	incl. 8.6 %	incl. 2.1 %

Table 2. Comparison between CPU times needed for advection with different numerical schemes – see section 4 for further details.

	Upwind scheme	Third order without flux limiter	Third order with flux limiter
Total CPU time	217 seconds	276 seconds	294 seconds
CPU time for advection	162 seconds (74.8%)	227 seconds (82.4%)	246 seconds (83.8%)
CPU time for flux computation	75 seconds (34.6%)	133 seconds (48.2%)	153 seconds (52.2%)

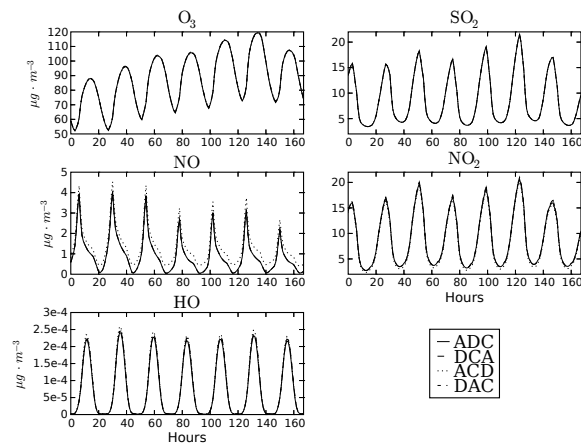


Figure 1. Time evolution of mean concentrations for several splitting sequences. Simulations in which chemistry comes before diffusion compute the same concentrations. On the contrary, simulation ACD shows differences.

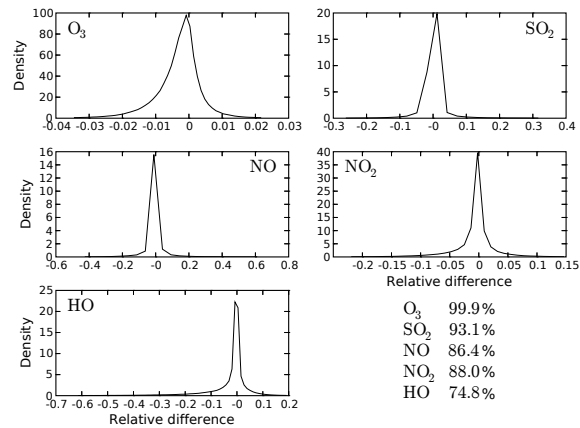


Figure 2. Splitting ADC versus DCA: relative frequency distribution of the distance Δ and agreement coefficients for the five species. Non negligible differences are observed, but the impact remains small.

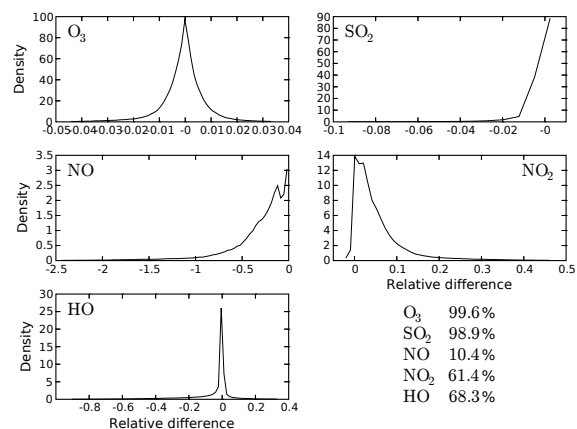


Figure 3. Splitting ADC versus ACD: relative frequency distribution of the distance Δ and agreement coefficients for the five species. Ozone and sulfur dioxide are slightly modified, while other species are sensitive to the numerical choice.

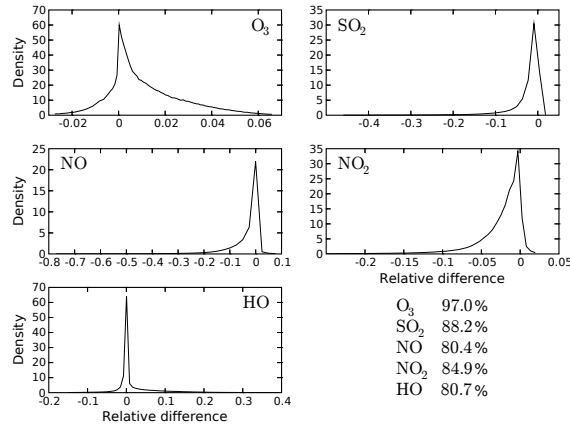


Figure 4. Simulations with ground boundary conditions included in diffusion versus in chemistry: relative frequency distribution of the distance Δ (see equation 3) and agreement coefficients for the five species. Ozone is not strongly modified while other species are affected.

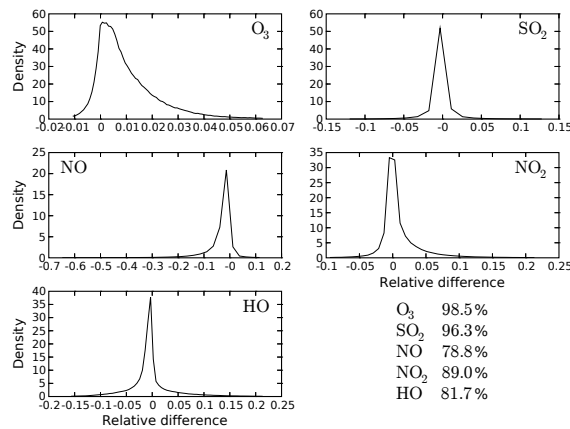


Figure 5. First-order splitting versus second-order splitting: relative frequency distribution of the distance Δ and agreement coefficients for the five species. Ozone and sulfur dioxide are barely modified; other species are sensitive to the numerical approximation.

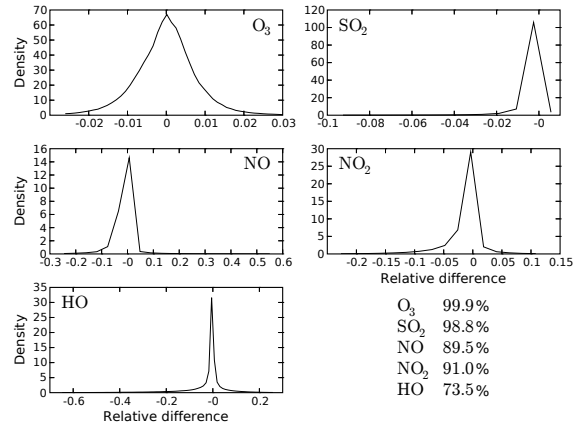


Figure 6. First-order splitting versus internal splitting: relative frequency distribution of the distance Δ and agreement coefficients for the five species. There is a low impact.

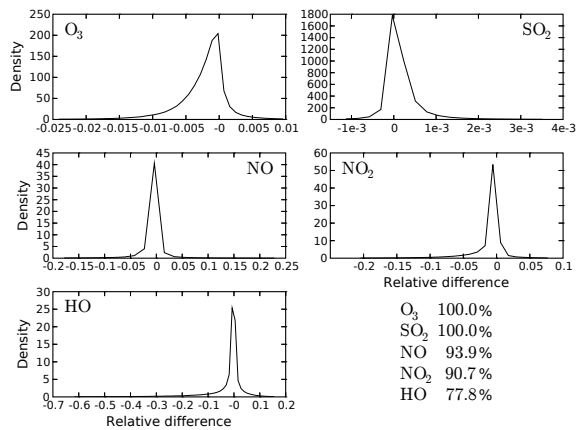


Figure 7. First-order splitting versus source splitting: relative frequency distribution of the distance Δ and agreement coefficients for the five species. There is a very low impact.

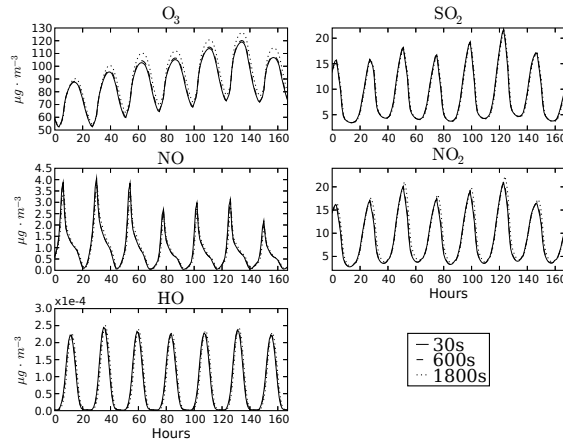


Figure 8. Time evolution of the spatial mean of concentrations computed with three time steps (30 s, 600 s and 1800 s). The simulation with 1800 s shows significant differences.

Table 3. Ratios between mean clipped concentrations (absolute value) and mean concentrations. Only species with a ratio above 0.005% are included.

Species	Ratio (%)	Species	Ratio (%)	Species	Ratio (%)
NO ₃	1.01	N ₂ O ₅	0.53	ETHP	0.52
OLND	0.52	OLNN	0.48	APIP	0.26
KETP	0.22	ETEP	0.06	HNO ₄	0.03
HC3P	0.02	XO ₂	0.02	XYLP	0.02
HC5P	0.02	HC8P	0.02	TOLP	0.02
OLTP	0.01	OLIP	0.01	ISOP	0.01

Table 4. Ratios between maximum clipped concentrations (absolute value) and mean concentrations. Only species with a ratio above 0.1 are included. Ratios are not in percent.

Species	Ratio	Species	Ratio	Species	Ratio
ETHP	121.39	APIP	95.49	KETP	60.00
NO ₃	15.58	OLND	13.53	ETEP	11.76
N ₂ O ₅	7.00	HC3P	6.04	XO ₂	4.54
OLNN	4.42	XYLP	4.09	TOLP	3.48
HC5P	3.36	HC8P	3.29	OLTP	2.12
OLIP	2.06	HNO ₄	1.39	CSLP	1.29
ISOP	0.70	PHO	0.70	MO ₂	0.22

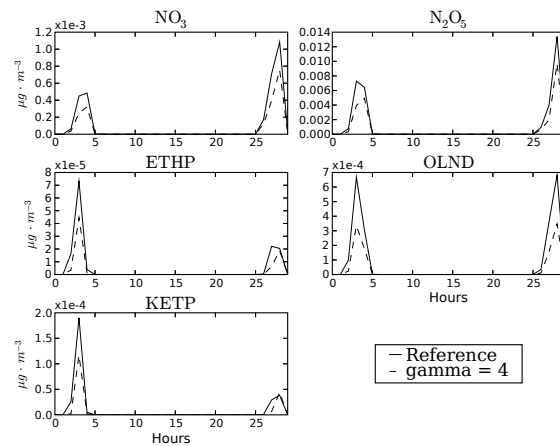


Figure 9. Time evolution of mean clipped concentrations for five species from Table 3 and 4. The reference simulation ($\gamma = 1 + \sqrt{2}/2$) is compared to the simulation with γ set to 4. The remaining hours have the same behavior. This indicates that $\gamma = 4$ is favorable at sunrise.

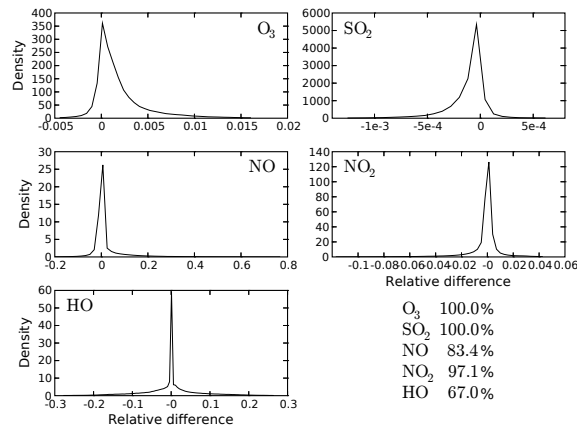


Figure 10. Reference simulation ($\gamma = 1 + \sqrt{2}/2$) versus simulation with γ set to 4: relative frequency distribution of the distance Δ and agreement coefficients for the five species. The impact is low.

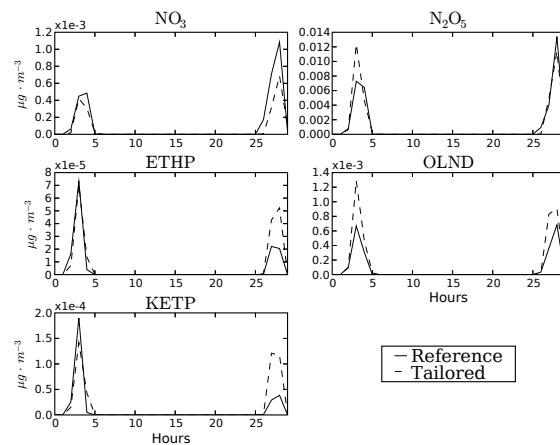


Figure 11. Time evolution of mean clipped concentrations for five species from Table 3 and 4. The reference simulation ($\gamma = 1 + \sqrt{2}/2$) is compared to the simulation with $\gamma \simeq \gamma^+(\beta)$. Only the first 30 hours are shown; the remaining hours have the same behavior.

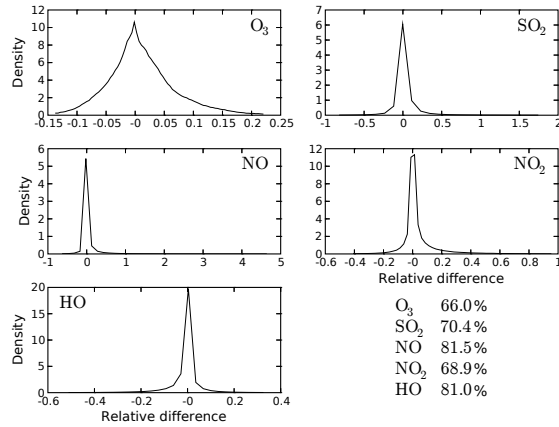


Figure 12. Third-order scheme with flux limiter versus upwind scheme: relative frequency distribution of the distance Δ and agreement coefficients for the five species.

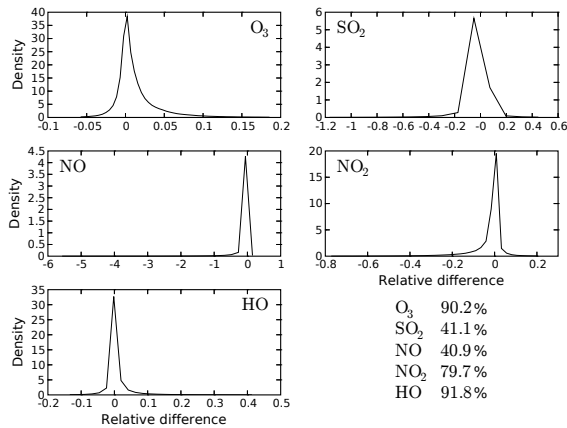


Figure 13. Third-order scheme with flux limiter versus third-order scheme without flux limiter: relative frequency distribution of the distance Δ and agreement coefficients for the five species.

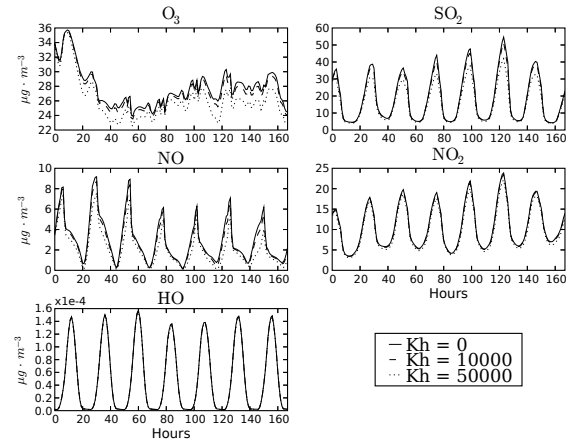


Figure 14. Time evolution of spatial standard deviations, with $K_h = 0$, $K_h = 10,000$ $\text{m}^2 \text{s}^{-1}$ and $K_h = 50,000$ $\text{m}^2 \text{s}^{-1}$.

Table 5. Summary of agreement coefficients for the main tests of the continental case.

The comparisons are ranked according to their ozone agreement coefficients.

Comparison	O ₃	SO ₂	NO	NO ₂	HO
$\Delta t = 600 \text{ s} / \Delta t = 1800 \text{ s}$	58.5	90.9	51.4	69.7	55.0
Reference / first order for advection	66.0	70.4	81.5	68.9	81.0
$K_h = 10\,000 \text{ m}^2 \text{ s}^{-1} / K_h = 50\,000 \text{ m}^2 \text{ s}^{-1}$	80.0	81.9	18.4	65.7	83.9
Reference / third order for advection	90.2	41.1	40.9	79.7	91.8
Bound. cond. in diffusion / bound. cond. in chemistry	97.0	88.2	80.4	84.9	80.7
$K_h = 10\,000 \text{ m}^2 \text{ s}^{-1} / K_h = 0 \text{ m}^2 \text{ s}^{-1}$	97.9	84.2	90.7	85.4	94.5
$\Delta t = 600 \text{ s} / \Delta t = 30 \text{ s}$	97.9	96.8	85.1	91.2	74.0
Reference / second order splitting	98.5	96.3	78.8	89.0	81.7
ADC / ACD	99.6	98.9	10.4	61.4	68.3
Reference / γ^+	99.7	100.0	94.6	97.7	97.9
ADC / DCA	99.9	93.1	86.4	88.0	74.8
Reference / internal splitting	99.9	98.8	89.5	91.0	73.5
Reference / $\gamma = 4$	100.0	100.0	83.4	97.1	67.0
Reference / source splitting	100.0	100.0	93.9	90.7	77.8

Table 6. Summary of agreement coefficients for the main tests of the regional case.

The comparisons are ranked according to their ozone agreement coefficients.

Comparison	O ₃	SO ₂	NO	NO ₂	HO
$\Delta t = 600 \text{ s} / \Delta t = 1800 \text{ s}$	40.9	60.4	76.9	34.8	16.5
ADC / ACD	64.5	90.0	11.7	33.2	22.5
First order splitting / second order splitting	83.4	66.5	19.4	71.2	17.9
Bound. cond. in diffusion / bound. cond. in chemistry	79.0	71.6	64.9	87.3	37.4
$\Delta t = 600 \text{ s} / \Delta t = 30 \text{ s}$	83.2	50.2	78.5	75.2	35.8
Reference / first order for advection	97.6	80.5	80.0	92.6	93.1
Reference / third order for advection	99.7	91.6	91.4	99.1	99.2
$K_h = 5 \text{ m}^2 \text{ s}^{-1} / K_h = 50 \text{ m}^2 \text{ s}^{-1}$	100.0	97.5	96.3	100.0	100.0
Reference / $\gamma = 4$	100.0	100.0	81.3	100.0	12.5
$K_h = 5 \text{ m}^2 \text{ s}^{-1} / K_h = 0 \text{ m}^2 \text{ s}^{-1}$	100.0	100.0	99.9	100.0	100.0
Reference / γ^+	100.0	100.0	100.0	100.0	100.0